Shear viscosity of quark matter at finite temperature under an external magnetic field

Seung-il Nam[1,*] and Chung-Wen Kao[2,†]

[1]*School of Physics, Korea Institute for Advanced Study (KIAS), Seoul 130-722, Korea*
[2]*Department of Physics, Chung-Yuan Christian University (CYCU), Chung-Li 32023, Taiwan*
(Received 31 March 2013; published 5 June 2013)

We employ the diluted instanton liquid model and the Green-Kubo formula to investigate the shear viscosity of the SU(2) light-flavor quark matter at finite temperature under an external strong magnetic field $e|\boldsymbol{B}| \sim m_\pi^2$. We apply the Schwinger method to calculate the effect of the external magnetic field. We find that the shear viscosity increases as temperature increases even beyond the transition temperature $T_0 = 170$ MeV if temperature-dependent model parameters are used. On the other hand, with temperature-independent ones the shear viscosity starts to drop when the temperature goes beyond T_0. Furthermore, we find that the presence of an external magnetic field will reduce the shear viscosity. However, this effect is almost negligible in the chiral-restored phase even for a very strong magnetic field, $e|\boldsymbol{B}| \approx 10^{20}$ gauss. We also compute the ratio of the shear viscosity and the entropy density η/s and our results are well compatible with the other theoretical results for a wide temperature range. We also provide the parametrization of the temperature-dependent ratio η/s from our numerical result as $\eta/s = 0.27 - 0.87/t + 1.19/t^2 - 0.28/t^3$ with $t \equiv T/T_0$ for $T = (100 \sim 350)$ MeV when $e|\boldsymbol{B}| = 0$.

DOI: 10.1103/PhysRevD.87.114003 PACS numbers: 12.38.−t, 12.40.−y, 52.27.Gr

I. INTRODUCTION

With the rapid development of heavy-ion collision (HIC) experiments at the Relativistic Heavy-Ion Collider at BNL and the Large Hadron Collider at CERN, the properties of quark-gluon plasma (QGP) have been intensively investigated. One of the most highlighted observations from those HIC experiments is that QGP behaves as an almost perfect fluid characterized by a small value of its shear viscosity. It has also been supported by several calculations based on the viscous hydrodynamics [1] or AdS/QCD models [2,3]. It implies that QGP is a strongly coupled system [4]. Furthermore, the value of the ratio of the shear viscosity and the entropy of QGP, $\frac{\eta}{s}$, is close to the Kovtun-Son-Starinets (KSS) bound [5]: $\frac{\eta}{s} \geq \frac{1}{4\pi}$. The viscous hydrodynamic simulation for the elliptic flow v_2 with the Monte Carlo (MC)-Glauber initial condition reproduces the Au + Au collision data with $\frac{\eta}{s} = \frac{1}{4\pi}$. On the contrary, the value $\frac{\eta}{s} \approx \frac{1}{2\pi}$ must be used to reproduce the experimental data if the MC Kharzeev-Levin-Nardi initial condition is adopted [1,6]. It indicates that the different initial conditions of the hydrodynamic simulations give different values of the shear viscosity. It is also worth noting that in the current hydrodynamic simulations, the value of the shear viscosity is always to be assumed to be independent of temperature. To extract a more realistic value of the shear viscosity from the hydrodynamical simulations, one needs to know the temperature dependence of the shear viscosity. In addition, the initial quantum fluctuations, such as the color-charge fluctuation, also cause an uncertainty in the extracted value of the shear viscosity of QGP. [7]. For a recent status for the shear viscosity, one may refer to Refs. [8,9].

The shear viscosity is able to be theoretically investigated by the Green-Kubo formula in the linear response theory [10–20]. Since QGP is a strongly coupled system, its properties can only be studied via nonperturbative methods in principle, such as low-energy effective QCD-like models or lattice QCD (LQCD) simulations. From the effective models, such as the Nambu-Jona-Lasinio (NJL) model, the shear viscosity has been scrutinized extensively as a function of temperature (T) and/or quark chemical potential (μ) [11,17,19]. The shear viscosity has also been studied by LQCD simulations [21], dissipative hydrodynamics [16,18], chiral perturbation theory (χPT) [12], perturbative QCD (pQCD) [13], and holographic models [2,3,22].

In addition to the shear viscosity of QGP, the effects of the external magnetic field produced in the peripheral HIC experiments have also attracted much attention [23]. Although the produced magnetic field is reduced by a factor $\sim 10^4$ after a short time ~ 3 fm/c [24], its strength is still very strong in the order of pion mass squared: $e|\boldsymbol{B}| \propto m_\pi^2 \sim 10^{18}$ gauss. Such a strength is comparable to the magnetic field of neutron stars. Recently people have speculated that a strong external magnetic field may generate the chiral magnetic effect and the chiral magnetic wave which will generate P-odd and CP-odd domains in QGP [25]. Furthermore, the chiral phase-transition temperature T_0 of the quark matter under a strong external magnetic field is enhanced, i.e., the magnetic catalysis [26]. It shows that the properities of the quark matter will be modified by the strong external magnetic field. Hence it is interesting to study the impact of the external magnetic field on the shear viscosity of QGP.

*sinam@kias.re.kr
†cwkao@cycu.edu.tw

In this article, we investigate the shear viscosity of the SU(2) light-flavor quark matter at finite temperature under a strong magnetic field. For this purpose, we employ the dilute instanton liquid model (DLIM) for the light-flavor SU(2) sector [27,28]. This model manifests the nontrivial quark-instanton interactions via the quark zero mode, resulting in the natural UV regulator by construction. Since we are interested in the system at finite temperature, we modify the DLIM parameters, such as the average inter(anti)instanton distance ($\bar{R}$) and (anti)instanton size ($\bar{\rho}$), using the caloron solution for the Yang-Mills equation with the trivial holonomy, i.e., the Harrington-Shepard caloron [29,30]. By computing $\bar{R}$ and $\bar{\rho}$ as functions of T with the caloron solution, we observe that they both decrease as temperature increases [30,31]. At $T \approx T_0$, where T_0 indicate the chiral phase-transition temperature, there appear about 10% decreases in $\bar{R}$ and $\bar{\rho}$ in comparison to their values at zero temperature. Using these results and the thermodynamic potential of DLIM, we show that the chiral phase transition is of second order ($T_0 \approx 166$ MeV) and the crossover ($T_0 \approx 170$ MeV) in the chiral limit and the finite-current quark mass case, respectively. It reproduces the correct universality class of the chiral restoration patterns. Since the quark chemical potential is expected to be small inside QGP created in HIC experiments, we choose $\mu = 0$ throughout the present work. As mentioned above, the Green-Kubo formula is employed to compute the shear viscosity in terms of a quark spectral function [11]. We construct a quark spectral function with a finite width $\Lambda \sim 1/\bar{\rho}$ motivated by the instanton physics. The external magnetic-field effect is calculated by the Schwinger method [32–34].

The numerical results for the shear viscosity are given as functions of temperature as well as the strength of the external magnetic field with the *temperature-dependent parameters*, $\bar{\rho}(T)$ and $\bar{R}(T)$ (TDP), and the *temperature-independent parameters*, $\bar{\rho}(0)$ and $\bar{R}(0)$ (TIP). With TIP, the shear viscosity increases as temperature increases up to T_0, then decreases smoothly. On the contrary, the shear viscosity keeps increasing beyond T_0 for TDP. We also observe the tendency for the external magnetic field to reduce the shear viscosity due to the enhancement of the SBχS, i.e., the magnetic catalysis. In the chiral limit, the magnetic-field effect on the shear viscosity vanishes when T goes beyond T_0. This is why the magnetic field effect is proportional to the constituent quark mass squared in our model, and the constituent quark mass vanishes when the system is in the chiral restored phase. However, in the finite quark-mass case, we observe that the shear viscosity continues to be reduced by the presence of the magnetic field even for $T > T_0$, but this effect fades away gradually from $T \approx 220$ MeV. In general, the effect from the magnetic field on the shear viscosity is less than 10% for $e|\boldsymbol{B}| \lesssim 100 m_\pi^2 \approx 10^{20}$ gauss.

We also present our result for the ratio of the shear viscosity and the entropy density η/s as a function of temperature and the strength of the external magnetic field. We find that η/s decreases smoothly and approaches the KSS bound for TDP, whereas the TIP result undershoots the bound. Moreover, the effects from the magnetic field become almost negligible beyond T_0, although the effects are still visible below T_0. We also compare our result for η/s with other theoretical estimations from the NJL model, LQCD, and χPT, resulting in qualitatively good agreement. Typical values for the shear viscosity at $T = T_0$ are given as $\eta = 0.02\ \mathrm{GeV}^3$ and $\eta/s = 0.29$ from the present model for $T = (100 \sim 350)$ MeV and $e|\boldsymbol{B}| = 0$.

The present work is organized as follows. In Sec. II, we introduce our theoretical framework for computing the shear viscosity of quark matter. The numerical results and relevant discussions are given in Sec. III, and the final section is devoted to the summary and future perspective.

II. THEORETICAL FRAMEWORK

In this section we briefly introduce our theoretical framework, including the Green-Kubo formula, the finite-width quark spectral function, the Schwinger method, and the DLIM thermodynamic potential.

A. Shear viscosity at finite temperature

The static shear viscosity η is defined according to the Green-Kubo formula [11],

$$\eta = -\frac{\partial}{\partial\omega}\,\mathrm{Im}[\Pi^{\eta}_{\mathrm{R}}(\omega)]|_{\omega=+0}, \tag{1}$$

where Π^{η}_{R} stands for the retarded (R) quark correlation function and ω is the frequency of the system. The retarded correlation function is related to the correlation function as follows:

$$\Pi^{\eta}_{\mathrm{R}}(\omega) = \Pi^{\eta}(i\omega_{\mathrm{M}})|_{i\omega_{\mathrm{M}}\to\omega+i\epsilon}. \tag{2}$$

Here ω_{M} is the fermionic Matsubara (M) frequency. Π^{η} is the time-ordered tensor current correlator,

$$\begin{aligned}\Pi^{\eta}(i\omega_{\mathrm{M}}) &= -\int_0^{1/T} d\tau e^{-i\omega_{\mathrm{M}}\tau}\\ &\quad\times\int d\boldsymbol{r}\langle 0|\mathcal{T}[J_{xy}(\boldsymbol{r},\tau), J_{xy}(0,0)]|0\rangle,\\ J_{xy} &= \frac{i}{2}[\bar{\psi}(\gamma_y\partial_x\psi) - (\partial_x\bar{\psi})\gamma_y\psi],\end{aligned} \tag{3}$$

where τ and ψ stand for the Euclidean time and the quark field, respectively. T denotes the temperature. One can evaluate Π^{η} with the full quark propagator S by using the fermionic Matsubara formula with $\omega_n = (2n+1)\pi T$,

$$\Pi^{\eta}(i\omega_{\mathrm{M}}) = T\int\frac{d^3\boldsymbol{k}}{(2\pi)^3}\sum_{n=\infty}^{\infty}\mathrm{Tr}_{c,f,\gamma}[k_x\gamma_y S(i\omega_{\mathrm{M}}+i\omega_n,\boldsymbol{k})k_x\gamma_y S(i\omega_n,\boldsymbol{k})]$$
$$= -\oint\frac{dz}{2\pi i}\int\frac{d^3\boldsymbol{k}}{(2\pi)^3}n_F(z)\,\mathrm{Tr}_{c,f,\gamma}[k_x\gamma_y S(i\omega_{\mathrm{M}}+z,\boldsymbol{k})k_x\gamma_y S(z,\boldsymbol{k})]. \tag{4}$$

The trace runs over the color (c), flavor, (f), and Lorentz (γ) indices. From the first line to the second line in Eq. (4), we have employed the fact that the poles of the Fermi-Dirac distribution,

$$n_F(z) = \frac{1}{1+e^{z/T}}, \tag{5}$$

are located at $z = i(2n+1)\pi T$. The relation between the free-quark spectral function ρ_0 and the quark propagator is given as

$$S(k_0,\boldsymbol{k}) = \int_{-\infty}^{\infty}\frac{d\omega}{2\pi}\frac{\rho_0(\omega,\boldsymbol{k})}{k_0-\omega}. \tag{6}$$

Hence we express the shear viscosity in terms of the quark spectral function $\rho_0(k)$,

$$\eta = -\frac{N_cN_f}{2}\lim_{\omega\to+0}\int\frac{dk_0}{2\pi}\frac{d^3\boldsymbol{k}}{(2\pi)^3}\frac{[n_F(k_0+\omega)-n_F(k_0)]}{\omega}k_x^2\,\mathrm{Tr}_{\gamma}[\rho_0(k_0+\omega,\boldsymbol{k})\gamma_y\rho_0(k_0,\boldsymbol{k})\gamma_y]$$
$$= -\frac{N_cN_f}{2}\int\frac{dk_0}{2\pi}\frac{d^3\boldsymbol{k}}{(2\pi)^3}n'_F(k_0)k_x^2\,\mathrm{Tr}_{\gamma}[\rho_0(k_0,\boldsymbol{k})\gamma_y\rho_0(k_0,\boldsymbol{k})\gamma_y]. \tag{7}$$

Here $n'_F = \frac{\partial n_F(z)}{\partial z}$. If we adopt the spectral function associated with the free-quark propagator with a current quark mass m given in Ref. [35], then

$$\rho_0(\omega,\boldsymbol{k}) = 2\pi\mathrm{sgn}[\omega](\gamma_0\omega - \boldsymbol{\gamma}\cdot\boldsymbol{k}+m)\delta(\omega^2-\boldsymbol{k}^2-m^2). \tag{8}$$

This quark spectral function satisfies the normalization condition $\frac{1}{2\pi}\int\rho(\omega,\boldsymbol{k})d\omega = \gamma_0$ [11] as shown in the Appendix. Because of the δ function in the spectral function in Eq. (8), the shear viscosity for the free quark at the mean-field level becomes zero, i.e., $\lim_{\epsilon\to0}\int d\omega f(\omega)\delta(\omega+\epsilon)\delta(\omega) = 0$ as long as $f(\omega)$ is a regular function. To overcome this difficulty, we introduce a finite width for the quark spectral function, as in Refs. [11,17]. Thus, we replace the delta function in Eq. (8) with a Gaussian functions with a finite width,

$$\delta(\omega^2-\boldsymbol{k}^2-m^2) = \delta(\omega^2-E^2)\to\frac{1}{2\sqrt{2\pi}E_{\boldsymbol{k}}\Lambda}\left[\exp\left[-\frac{(\omega-E_{\boldsymbol{k}})^2}{2\Lambda^2}\right]+\exp\left[-\frac{(\omega+E_{\boldsymbol{k}})^2}{2\Lambda^2}\right]\right]\equiv\mathcal{F}(\omega,\boldsymbol{k}),$$
$$E_{\boldsymbol{k}} = \sqrt{\boldsymbol{k}^2+M_{\boldsymbol{k}}^2},\qquad M_{\boldsymbol{k}} = M_0(T)\left[\frac{2}{2+\bar{\rho}^2(T)\boldsymbol{k}^2}\right]^{2n}. \tag{9}$$

Note that $\Lambda\sim1/\bar{\rho}$ is the width for the Gaussian function.

It is worth mentioning that $M_{\boldsymbol{k}}$ presents the nonlocal (momentum-dependent) interaction of the quarks. In the instanton model, the Dirac equation for a quark can be solved in the presence of the (anti)instanton ensemble [27,28]. Assuming that the fermionic zero mode dominates the low-energy phenomena, one can obtain the zero-mode solution and perform the Fourier transform of this solution, which results in the momentum-dependent effective quark mass. It is also called the constituent quark mass since essentially it is same as the quark mass in the naive constituent quark models. Physically, this momentum dependence can be understood by the nontrivial interactions between the quarks and the instantons via the zero mode, i.e., the delocalization of the quark zero mode [27]. The parameter n in Eq. (9) will be determined by reproducing the correct value of the chiral condensate. Note that the constituent quark mass at zero virtuality M_0 and average (anti)instanton size $\bar{\rho}$ are functions of temperature here. They will be discussed in detail later. Combining Eqs. (8) and (9), we arrive at the expression for the finite-width (FW) quark spectral function,

$$\rho_0\to\rho_{\mathrm{FW}}(\omega,\boldsymbol{k}) = 2\pi\mathrm{sgn}[\omega](\gamma_0\omega-\boldsymbol{\gamma}\cdot\boldsymbol{k}+\bar{M}_{\boldsymbol{k}})\mathcal{F}(\omega,\boldsymbol{k}). \tag{10}$$

Note that the current quark mass m has been replaced by the momentum-dependent effective quark mass $\bar{M}_{\boldsymbol{k}} = M_k + m$ to regulate the quark-loop integral. ρ_{FW} also satisfies the normalization condition for the quark spectral function as shown in the Appendix. The chiral condensate can be related to the spectral function in Minkowski space,

$$\langle\bar{q}q\rangle = -iN_c\int\frac{d^4p}{(2\pi)^4}\,\mathrm{Tr}_\gamma[S(p_0,\boldsymbol{p})] = iN_c\int\frac{d\omega d^4p}{(2\pi)^5}\,\mathrm{Tr}_\gamma\left[\frac{\rho_{\mathrm{FW}}(\omega,\boldsymbol{p})}{p_0-\omega}\right]. \tag{11}$$

Performing the Wick rotation for the temporal direction and integrating over $(\omega, ik_0, \boldsymbol{k})$, one is led to

$$\langle\bar{q}q\rangle = -8N_c\int\frac{d^4k}{(2\pi)^4}\int_0^\infty d\omega\frac{\bar{M}_{\boldsymbol{k}}\mathcal{F}(\omega,\boldsymbol{k})}{k_0^2+\omega^2}. \tag{12}$$

The vacuum values for $\bar{\rho}$ and $\bar{R}$ were estimated by the LQCD simulation [$(\bar{\rho},\bar{R})\approx(0.36, 0.89)$ fm] [36], the variational method [$(\bar{\rho},\bar{R})\approx(0.35, 0.95)$ fm] [27], and the phenomenological way [$(\bar{\rho},\bar{R})\approx(1/3, 1)$ fm] [37]. Among them, we choose the phenomenological values for our numerical calculation. Note that the value of M_0 at $T = 0$ is determined by reproducing various low-energy constants with the instanton parameters [27]. For instance, using $M_0 \approx 300$ MeV, one obtains the pion weak-decay constant $F_\pi \approx 93$ MeV, which is very close to its empirical value, $F_\pi = 93.2$ MeV [38]. Employing these vacuum values for M_0, $\bar{\rho}$, and $\bar{R}$ to reproduce the empirical value of the chiral condensate $\langle\bar{q}q\rangle \approx -(250\ \mathrm{MeV})^3$ in the chiral limit [27], we choose $n = 2$ in Eq. (9). This choice gives $\langle\bar{q}q\rangle \approx -(239\ \mathrm{MeV})^3$ from Eq. (12) in the finite current quark-mass case, which is comparable to the empirical value. Throughout the present work we will use $n = 2$.

Taking into account all the ingredients discussed so far, we arrive at the following concise expression for the shear viscosity:

$$\eta = \frac{N_cN_f}{2\pi^2T}\int dk_0d^3\boldsymbol{k}n_F(k_0)[n_F(k_0)-1] \times\mathcal{F}^2(\omega,\boldsymbol{k})k_x^2[2k_y^2+k^2-M_{\boldsymbol{k}}^2]. \tag{13}$$

B. Temperature dependencies of $\bar{\rho}$ and $\bar{R}$

Here we explain briefly how to modify $\bar{\rho}$ and $\bar{R}$ as functions of T. Details can be found in Ref. [31]. This derivation uses the caloron distribution with trivial holonomy, i.e., the Harrington-Shepard caloron [29,30]. An instanton distribution function for arbitrary N_c and N_f can be written with a Gaussian suppression factor as a function of T and an arbitrary instanton size ρ for pure Yang-Mills theory [30],

$$d(\rho,T) = \underbrace{C_{N_c}\Lambda_{\mathrm{RS}}^b\hat{\beta}^{N_c}}_{\mathcal{C}}\rho^{b-5}\exp[-(A_{N_c}T^2+\bar{\beta}\gamma n\bar{\rho}^2)\rho^2]. \tag{14}$$

We note that the CP-invariant vacuum was taken into account in Eq. (14), and we assumed the same analytical form of the distribution function for both the instanton and anti-instanton. Note that the instanton number density (packing fraction) $N/V \equiv n \equiv 1/\bar{R}^4$ and $\bar{\rho}$ have been taken into account as functions of T implicitly. For simplicity, we take the numbers of the anti-instanton and instanton to be the same, i.e., $N_I = N_{\bar{I}} = N$. We also assigned the constant factor on the right-hand side of the above equation as $\mathcal{C}$ for simplicity. The abbreviated notations are also given as

$$\hat{\beta} = -b\ln[\Lambda_{\mathrm{RS}}\rho_{\mathrm{cut}}],\quad \bar{\beta} = -b\ln[\Lambda_{\mathrm{RS}}\langle R\rangle],$$
$$C_{N_c} = \frac{4.60e^{-1.68\alpha_{\mathrm{RS}}Nc}}{\pi^2(N_c-2)!(N_c-1)!},\quad A_{N_c} = \frac{1}{3}\left[\frac{11}{6}N_c-1\right]\pi^2,$$
$$\gamma = \frac{27}{4}\left[\frac{N_c}{N_c^2-1}\right]\pi^2,\quad b = \frac{11N_c-2N_f}{3}. \tag{15}$$

Note that we defined the one-loop inverse charges $\hat{\beta}$ and $\bar{\beta}$ at certain phenomenological cutoffs ρ_{cut} and $\langle R\rangle \approx \bar{R}$. Λ_{RS} denotes a scale depending on the renormalization scheme, whereas V_3 stands for the three-dimensional volume. Using the instanton distribution function in Eq. (14), we are able to compute the average value of the instanton size $\bar{\rho}^2$ as follows [39]:

$$\bar{\rho}^2(T) = \frac{\int d\rho\rho^2d(\rho,T)}{\int d\rho d(\rho,T)} = \frac{[A_{N_c}^2T^4+4\nu\bar{\beta}\gamma n]^{\frac{1}{2}}-A_{N_c}T^2}{2\bar{\beta}\gamma n}, \tag{16}$$

where $\nu = (b-4)/2$. It can be easily shown that Eq. (16) satisfies the following asymptotic behavior [39]:

$$\lim_{T\to0}\bar{\rho}^2(T) = \sqrt{\frac{\nu}{\bar{\beta}\gamma n}},\qquad \lim_{T\to\infty}\bar{\rho}^2(T) = \frac{\nu}{A_{N_c}T^2}. \tag{17}$$

Here, the second relation of Eq. (17) indicates a correct scale-temperature behavior at high T, i.e., $1/\bar{\rho} \approx \Lambda \propto T$. Substituting Eq. (16) into Eq. (14), the caloron distribution function can be evaluated further,

$$d(\rho,T) = \mathcal{C}\rho^{b-5}\exp[-\mathcal{F}(T)\rho^2],$$
$$\mathcal{F}(T) = \frac{1}{2}A_{N_c}T^2+\left[\frac{1}{4}A_{N_c}^2T^4+\nu\bar{\beta}\gamma n\right]^{\frac{1}{2}}. \tag{18}$$

The instanton packing fraction n can be computed self-consistently using the following equation:

$$n^{\frac{1}{\nu}}\mathcal{F}(T) = [\mathcal{C}\Gamma(\nu)]^{\frac{1}{\nu}}, \tag{19}$$

where we replaced $NT/V_3 \to n$, and $\Gamma(\nu)$ stands for the Gamma function with an argument ν. Note that $\mathcal{C}$ and $\bar{\beta}$ can be determined by Eqs. (16) and (19) with the vacuum values for $n \approx (200\ \mathrm{MeV})^4$ and $\bar{\rho} \approx (600\ \mathrm{MeV})^{-1}$: $\mathcal{C} \approx 9.81\times10^{-4}$ and $\bar{\beta} \approx 9.19$. Finally, in order to estimate the T dependence of M_0, one needs to consider the normalized distribution function, defined as follows:

$$d_N(\rho,T) = \frac{d(\rho,T)}{\int d\rho d(\rho,T)} = \frac{\rho^{b-5}\mathcal{F}^\nu(T)\exp[-\mathcal{F}(T)\rho^2]}{\Gamma(\nu)}. \tag{20}$$

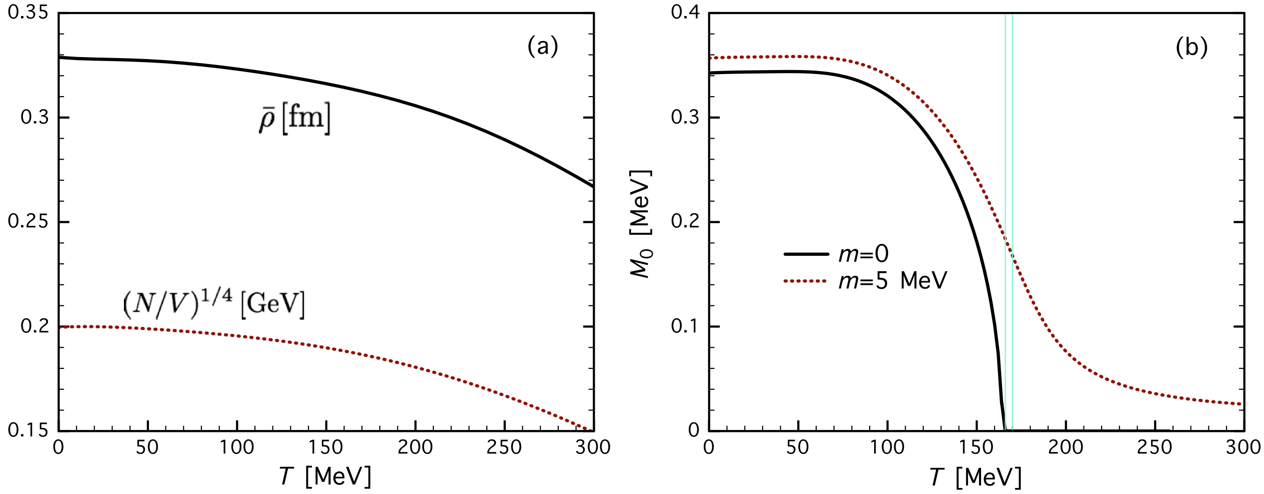

FIG. 1 (color online). Average (anti)instanton size $\bar{\rho} \approx 1/\Lambda$ [fm] and (anti)instanton packing fraction $(N/V)^{1/4}$ [GeV] as functions of T, computed from the Harrington-Shepard caloron distribution [29,30] in panel (a). Effective quark mass at zero virtuality, M_0 computed from Eq. (23) as functions of T for $m = 0$ (solid) and $m = 5$ MeV (dot), signaling the second-order and crossover chiral phase transitions, respectively, in panel (b). The vertical lines indicate the chiral phase-transition temperatures $T_0 = (166, 170)$ MeV for $m = (0, 5)$ MeV.

Here, the subscript N denotes the normalized distribution. For brevity, we want to employ the large-N_c limit to simplify the expression for $d_N(\rho, T)$. In this limit, $d_N(\rho, T)$ can be approximated as a δ function,

$$\lim_{N_c\to\infty} d_N(\rho, T) = \delta[\rho - \bar{\rho}(T)]. \tag{21}$$

The numerical result for $\bar{\rho}(T)$ is given in panel (a) in Fig. 1. This result shows that the average (anti)instanton size smoothly decreases with respect to temperature. It indicates that the instanton ensemble becomes diluted and the nonperturbative effects via the quark-instanton interactions are diminished as T increases. At $T = (150 \sim 200)$ MeV, which is close to the chiral phase-transition temperature, the instanton size decreases by about $(10 \sim 20)\%$ in comparison to its value at $T = 0$. Considering that the instanton size corresponds to the scale parameter of the model, i.e., the UV cutoff mass, $\bar{\rho} \approx 1/\Lambda$, the temperature-dependent cutoff mass is a clearly distinctive feature in comparison to other low-energy effective models, such as the NJL model. In addition, we also show the temperature dependence of the average (anti)instanton number density or (anti)instanton packing fraction, N/V, in panel (a) of Fig. 1. Similarly, the instanton number density decreases as temperature increases since the instanton ensemble is diluted. We will use these two temperature-dependent quantities for computing the shear viscosity in Eq. (13).

C. Temperature dependencies of the effective quark mass M_0 and the entropy density s

As in Ref. [31], the leading $1/N_c$ contribution of the DLIM thermodynamic potential per volume at zero quark chemical potential can be written as follows:

$$\Omega_{\rm LIM} = \frac{N}{V}\left[1 - \ln\frac{N}{\lambda V \mathrm{M}}\right] + 2\sigma^2 - 2N_cN_f\int_0^\infty \frac{d^3\boldsymbol{k}}{(2\pi)^3}[E_{\boldsymbol{k}} + 2T\ln[1 + e^{-\frac{E_{\boldsymbol{k}}}{T}}]], \tag{22}$$

where λ represents a Lagrange multiplier to exponentiate the effective quark-instanton action and M stands for an arbitrary mass parameter to make the argument for the logarithm dimensionless. σ stands for the isosinglet scalar meson field corresponding to the effective quark mass. In the large-N_c limit, we have the relation $2\sigma^2 = N/V$ [31]. The gap equation can be derived from Eq. (22) by differentiating $\Omega_{\rm LIM}$ by the Lagrange multiplier λ,

$$\frac{\partial \Omega_{\rm LIM}}{\partial \lambda} = 0 \to \frac{N_f}{\bar{M}_0}\frac{N}{V} - 2N_cN_f \times \int_0^\infty \frac{d^3\boldsymbol{k}}{(2\pi)^3} F_{\boldsymbol{k}}^4 \frac{M_0}{E_{\boldsymbol{k}}}\left[1 - \frac{2e^{-\frac{E_{\boldsymbol{k}}}{T}}}{1 + e^{-\frac{E_{\boldsymbol{k}}}{T}}}\right] = 0. \tag{23}$$

Note that one can write the instanton packing fraction in terms of the effective quark mass M_0 and $\bar{\rho}$ [27],

$$\frac{N}{V} = \frac{\mathcal{C}_0 N_c M_0^2}{\pi^2 \bar{\rho}^2}. \tag{24}$$

The value of $\mathcal{C}_0$ is in $(1/3 \sim 1/4)$ for $1/\bar{\rho} \approx 600$ MeV, $M_0 \approx (300 \sim 400)$ MeV, and $N/V \approx (200 \sim 260\ \mathrm{MeV})^4$ for vacuum [40]. We choose $\mathcal{C}_0 = 0.27$ to reproduce $M_0 = (340 \sim 350)$ MeV at $(T, \mu) = 0$ in the chiral limit. The numerical results for M_0 as a function of T are given in panel (b) of Fig. 1 for the zero and finite current quark mass: $m = 0$ (solid) and $m = 5$ MeV (dotted). These results indicate the correct universal patterns for the phase-transition pattern like those of the Ising model, i.e., the second-order chiral phase transition for the massless quark and the crossover for the finite quark mass. Here we choose the current quark mass to be about 5 MeV: $m_u \approx m_d \approx m = 5$ MeV. From these numerical results, the transition temperatures for the two cases are $T_0 \approx (166, 170)$ MeV for $m = (0, 5)$ MeV. The transition temperatures are indicated by the thin solid vertical lines in panel (b) of Fig. 1. Since we are interested in the ratio of the shear viscosity and the entropy density η/s, we derive the entropy density s as follows:

$$s \equiv -\frac{\partial \Omega_{\mathrm{LIM}}}{\partial T}. \tag{25}$$

From the effective thermodynamic potential in Eq. (22), we obtain the entropy density within the present model,

$$s \approx -\left(\frac{\partial}{\partial T}\frac{N}{V}\right)\left[1 - \ln\left(\frac{N}{V\Lambda^4}\right)\right] + 4N_cN_f \int \frac{d^3\boldsymbol{k}}{(2\pi)^3}\left\{\ln\left[1 + e^{-E_k/T}\right] + \frac{E_{\boldsymbol{k}}}{T} n_F(E_{\boldsymbol{k}})\right\}. \tag{26}$$

In deriving Eq. (26), we assume that $2\sigma^2 \approx N/V$ and $\lambda \mathrm{M} \approx \Lambda^4$ as in the leading $1/N_c$, since Λ is only the scale parameter of the present model. The logarithm term $\ln[\cdots]$ in the first square bracket on the right-hand side of Eq. (26) gives a small contribution to the entropy density. As understood in panel (a) of Fig. 1, the (anti) instanton number density N/V is a function of temperature, so that its derivative with respect to T in the first term on the right-hand side of Eq. (26) is finite in general within the present model. The detailed calculations for these quantities will be given in a separate article [41].

D. Shear viscosity under a strong external magnetic field

Here, we briefly discuss how to calculate the influence of an external magnetic field field on the quark matter. Following the Schwinger method, we apply the minimal gauge substitution to the covariant derivative, $i\partial_\mu \to iD_\mu = i\partial_\mu + ie_qA_\mu$. By doing this, the momentum-dependent effective quark mass can be expanded in terms of the electric charge of the quark, which gives us the following expression for $\mathcal{O}(e_q)$ [42]:

$$\begin{aligned} M_{\boldsymbol{k}} &\to M_{\boldsymbol{k}} + \frac{i}{2}(\sigma \cdot F)\tilde{M}_{\boldsymbol{k}}, \\ \tilde{M}_{\boldsymbol{k}} &= -\frac{32M_0\bar{\rho}^2}{(2 + \bar{\rho}^2\boldsymbol{k}^2)^5}, \quad \text{for } n = 2. \end{aligned} \tag{27}$$

For convenience, we choose the specific configuration for the external magnetic field to be

$$\boldsymbol{B} = (B_x, B_y, B_z) = (0, B_0 \sin\theta_B, B_0 \cos\theta_B), \tag{28}$$

where θ_B is an arbitrary angle. It has been verified that choosing an arbitrary field configuration does not generate any qualitative difference. Considering the fact that 1 G $= 1.95 \times 10^{-14}$ MeV^2 in the natural units and $m_\pi^2 \approx 10^{18}$ G in terms of the pion mass $m_\pi \approx 140$ MeV, it is quite convenient to employ the following parametrization for the magnetic field: $eB_0 = n_B m_\pi^2$. As for $n_B = 1$, the strength of the magnetic field is comparable to that of the magnetar. If n_B becomes about $(10 \sim 100)$, it can be compared to the strong magnetic field observed at the peripheral heavy-ion collisions at Relativistic Heavy-Ion Collider [24].

Combining all these ingredients, we have a simple expression for the shear viscosity as a function of (T, B_0) up to $\mathcal{O}(e_q^2)$,

$$\eta(T, B_0) = \sum_{q=u,d} \frac{N_c}{2\pi^2 T} \int dk_0 d^3\boldsymbol{k} n_F(k_0)[n_F(k_0) - 1] \times \mathcal{F}^2(k)k_x^2[2k_y^2 + k^2 - M_{\boldsymbol{k}}^2 + 3(e_qB_0)^2\tilde{M}_{\boldsymbol{k}}^2], \tag{29}$$

where the summation runs over the light flavors u and d. Corresponding electrical quark charges are $(e_u, e_d) = (+2/3, -1/3)e$, in which e denotes the unit electrical charge $e = \sqrt{4\pi\alpha_{\mathrm{EM}}}$ in the natural unit. Note that the magnetic field effect comes only from $3(e_qB_0)^2\tilde{M}_{\boldsymbol{k}}^2$, which is proportional to $M_0^2(T)$ as shown in Eq. (27).

III. NUMERICAL RESULTS AND DISCUSSIONS

In this section, we present and discuss our numerical results of the shear viscosity. In Fig. 2, the shear viscosity is presented as a functions of T under the external magnetic field $B_0 = n_B m_\pi^2$ in the chiral limit (a) and in the case of finite current quark mass $m = 5$ MeV (b). The thick and thin lines indicate those with T-dependent parameters and T-independent parameters, respectively. The vertical lines shown in both panels denote the transition temperatures T_0.

For TDP, the shear viscosity starts from zero and keeps increasing as T increases, whereas it decreases beyond T_0 for TIP. This observation suggests that the T dependencies of the parameters of our model generate significant effects on the shear viscosity. It is worth noting that similar behavior was also observed in the NJL-model calculation [11], although they considered a small quark chemical potential $\mu = 10$ MeV and they treated the finite width for the quark spectral function as a free parameter. The difference between the TDP and TIP cases can be explained as follows. A system with weaker interactions between its constituents has a larger value of the shear viscosity. In the TDP case, the interquark interactions become weaker, indicated by the fact that the DLIM parameters decrease as T increases. However, in the TIP case, the interquark interactions remain strong enough even when T goes beyond T_0. This results in the decrease of the shear viscosity with respect to T.

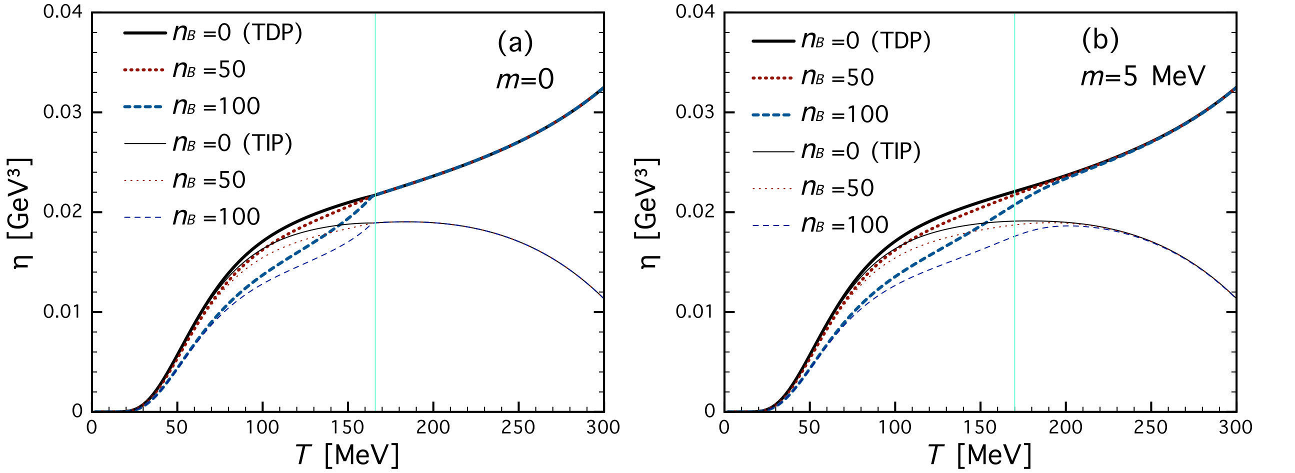

FIG. 2 (color online). (a) Shear viscosities η in the chiral limit as functions of T for different strengths for the *static* external magnetic field $eB_0 = n_B m_\pi^2$ for $n_B = 0$ (solid), 50 (dotted), and 100 (dashed) with the T-dependent parameters (TDP, thick) and T-independent parameters (TIP, thin). (b) The same curves with $m = 5$ MeV. The vertical lines indicate the chiral phase-transition temperatures $T_0 = (166, 170)$ MeV for the (left, right) panels.

Furthermore, the shear viscosity becomes smaller under the strong magnetic field for both cases of $m = (0, 5)$ MeV. This tendency can be explained by the enhancement of SBχS, in terms of the magnetic catalysis [43]. In our theoretical framework, the magnetic field contribution is proportional to $\tilde{M}_{\boldsymbol{k}}^2 \propto M_0^2(T)$, as shown in Eqs. (27) and (29). M_0 is the order parameter of the chiral restoration phase transition. Hence, the magnetic-field contribution disappears beyond T_0 in the chiral limit as shown in panel (a) of Fig. 2, due to the nature of the second-order chiral phase transition shown in panel (b) of Fig. 1. The magnetic-field effect remains finite even beyond T_0 in the case of the finite current quark mass as in panel (b) of Fig. 2. This is due to the crossover pattern of the chiral restoration there. At very high temperatures such as $T \gtrsim 220$ MeV, the magnetic-field effect almost vanishes even in the finite current quark mass case. Near the transition temperature $T_0 \approx 170$ MeV, the shear viscosity becomes approximately $\eta \approx 0.02\ \mathrm{GeV}^3$ for all cases.

In the literature, the ratio of the shear viscosity and the entropy density η/s has been considered as an important physical quantity. Hence we also present our result for η/s here. First, in the left panel of Fig. 3, we depict the entropy density using Eq. (26) for TDP (solid) and TIP (dash).

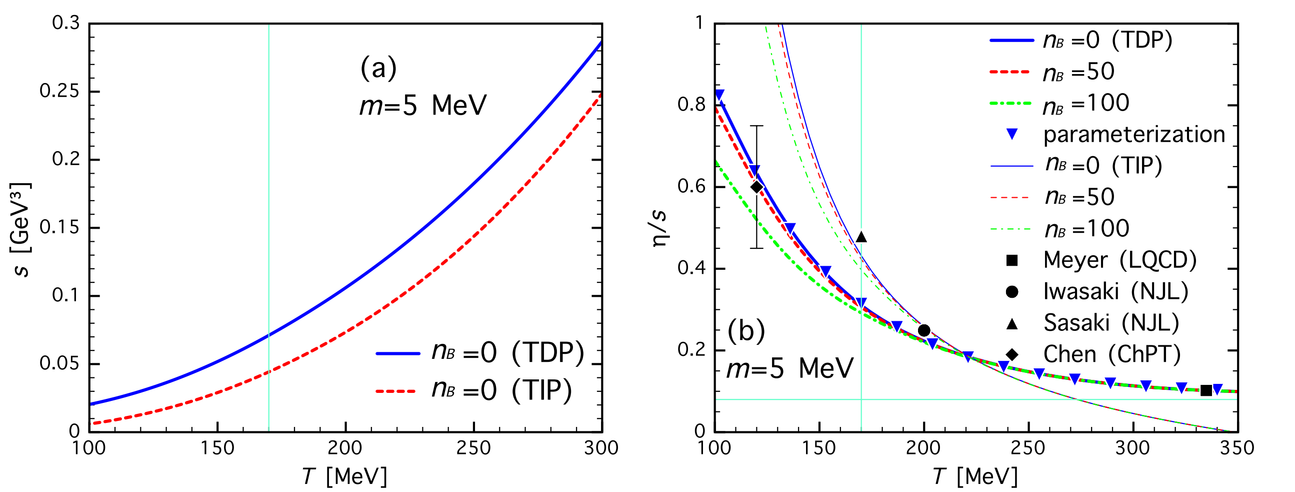

FIG. 3 (color online). (a) Entropy density s as a function of T for with the T-dependent parameters (TDP, thick) and T-independent parameters (TIP, thin). (b) The ratio of the shear viscosity and entropy density η/s in the same manner with the left panel, with different strengths of the external magnetic fields, $n_B = (0, 50, 100)$, given in the (solid, dash, dot-dash) lines. We also show the theoretical results from Meyer (LQCD) [21] (square), Iwasaki (NJL) [17] (circle), Sasaki (NJL) [19] (triangle), and Chen (χPT) [12] (diamond). The parametrization of the TDP curve for $n_B = 0$ in Eq. (30) is also given with the solid nabla. Detailed explanations for these theoretical values are given in the text. The vertical lines indicate the chiral phase-transition temperatures $T_0 = 170$ MeV for the (left, right) panels, while the horizontal one in the right panel stands for the lower bound of the QGP shear viscosity, i.e., the KSS bound $\eta/s = 1/(4\pi) \approx 0.08$.

Since we are interested only in the cases with the finite current quark mass, we choose $m = 5$ MeV, as mentioned before. We find that the value of s is smoothly increasing with respect to T for both cases. The result for TDP is always larger than for TIP. This can be easily explained by the fact that the first term on the right-hand side of Eq. (26) becomes zero for the TIP case. Note that here we set the external magnetic field to zero since we have verified that the magnetic field contribution to the entropy density is negligible.

In the right panel of Fig. 3, we have shown the numerical results for the ratio η/s as functions of T for TDP (thick) and TIP (thin), with different strengths of the magnetic field. The present model scale is about $\Lambda \approx 600$ MeV since it corresponds to the nonperturbative QCD region. Therefore, we confine our discussion to a temperature not much farther beyond the chiral transition, i.e., $T_{\max} = 350$ MeV. The magnetic field dependence of η/s comes only from the numerator η. The horizontal and vertical lines stand for the chiral transition temperature $T_0 = 170$ MeV and the KSS-bound value $\eta/s = 1/(4\pi) \approx 0.08$, respectively. The curves of η/s of the TDP case decrease smoothly and approach the KSS bound as T increases. Those for the TIP case behave similarly but decrease faster with respect to T. Note that the TIP curves undershoot the KSS bound at $T \approx 270$ MeV. This implies that it is necessary to take the temperature dependence of the model parameters into consideration. The effect of the magnetic field is sizable below the chiral transition, and then becomes negligible beyond T_0. Near the transition point, we observe only a few percent changes in the ratio η/s due to the magnetic field.

In the right panel of Fig. 3, the other theoretical estimations for the ratio η/s are also presented for comparison. In Ref. [21], the Monte Carlo simulation of the two-point correlations in the pure SU(3) gauge were been employed to compute the ratio with the nonperturbatively normalized operators. It gives $\eta/s = (0.134, 0.102)$ at $T = (1.65, 1.24)T_0$. This result is represented by the solid square. The TDP curves are well compatible with their value at $T \approx 335$ MeV, while the TIP curves undershoot the value.

The effective models such as the NJL model have also been used for estimating the ratio. In Ref. [17], it was reported that $\eta/s \approx (1/4\pi \sim 0.9)$ at $(T, \mu) = (200, 10)$ MeV, depending on the finite width of the quark spectral function. Averaging their values over the finite width, we have $\eta/s \approx 0.25$, and this is represented by the solid circle in the left panel of Fig. 3. It lies between the TDP and TIP curves. In a previous work with the same theoretical framework [11], the shear viscosity increases slowly with the larger quark chemical potential. Hence the depicted point in the right panel is supposed to be lowered at $\mu = 0$. Nevertheless, the change from $\mu = (10 \to 0)$ MeV will not be substantial in the present discussion.

Employing the NJL model, Ref. [19] explored the transport coefficients near the chiral phase transition. Their result of the ratio $\eta/s \approx 0.5$ at $T \approx 170$ MeV. This value is depicted in the right panel of Fig. 3 with the solid triangle. It is comparable with the TIP curves but it is larger than the TDP curves by about 50%. Note that the temperature dependencies of the η/s curves in Ref. [19] are similar to ours when $T < T_0$. However, their curves turn slightly upwards when $T \gtrsim T_0$ and are no longer similar to our results. In Ref. [12] they computed η/s by using χPT below the chiral transition temperature. They estimated η/s as a decreasing function of T with a typical value $\eta/s = 0.6$ at $T = 120$ MeV with 50% uncertainty. We depict this value with the solid diamond with the error bar in the right panel of Fig. 3. It matches with the TDP curves well. There are other theoretical estimations for η/s for the high-T ($T \gtrsim 450$ MeV) regions from LQCD and pQCD [13,14,44,45], and those results can not be reproduced in our model here. Their results are usually larger than ours by $(5 \sim 10)$ times. It is because of this that our model is essentially unapplicable at very high temperatures since the instanton physics becomes irrelevant there.

Finally, we provide a simple parametrization of the ratio η/s as a function of T. Since many theoretical approaches for the QGP dynamics have used a T-independent η/s value [1], this parametrization would help to construct more realistic models of QGP. Taking into account that the magnetic-field effects are negligible for $T > T_0$ as shown in the right panel of Fig. 3, we just parametrize the numerical result for $n_B = 0$. Employing a simple analytic form, one is led to

$$\frac{\eta}{s} = 0.27 - \frac{0.87}{t} + \frac{1.19}{t^2} - \frac{0.28}{t^3}, \quad T = (100 \sim 350\ \text{MeV}), \tag{30}$$

where we use the notation $t = T/T_0$ with $T_0 = 170$ MeV. In the right panel of Fig. 3, the values given according to Eq. (15) are denoted by the solid nabla symbols.

IV. SUMMARY AND FUTURE PERSPECTIVES

In summary, we have employed the diluted instanton liquid model and the Green-Kubo formula to investigate the shear viscosity of the SU(2) light-flavor quark matter at finite temperature under an external magnetic field. The effect of an external magnetic field has been calculated by the Schwinger method. Since the shear viscosity becomes zero when the free quark spectral function is adopted, we choose a quark spectral function with a finite width motivated by the instanton model. We use the chiral condensate value at zero temperature to determine the only free parameter in this quark spectral function. The important observations of our results are as follows.

(i) Our model is different from usual local-interaction models because several parameters in our model, such as the average instanton size and the inter-instanton distance, are subjected to temperature. Our treatment of these parameters is corroborated by the fact that our effective thermodynamic potential in the large-N_c limit generates the correct chiral restoration patterns, i.e., the second-order and the crossover phase transitions for $m = 0$ and $m \neq 0$, respectively.

(ii) We find that the external magnetic field reduces η due to the magnetic catalysis, i.e., the quarks are coupled more strongly in the presence of the magnetic field. This effect is sizable below the chiral transition temperature $T_0 = (166, 170)$ MeV for $m = (0, 5)$ MeV. However, it becomes negligible when the temperature goes beyond T_0. We also obtain a typical value for the shear viscosity near T_0, which is $\eta = 0.02\ \mathrm{GeV}^3$.

(iii) We observe that the T-dependent parameters, $\bar{\rho}(T)$ and $\bar{R}(T)$, play an important role beyond T_0, which causes η to continue to increase. In contrast, η starts to decrease after T_0, if the T-independent parameters are chosen. The ratio of the shear viscosity and the entropy density, η/s, has been computed in the finite current quark mass. It has been shown to be a monotonically decreasing function of $T = (100 \sim 350)$ MeV. Furthermore, we find that η/s undershoots the KSS bound, $\eta/s = 1/(4\pi)$, for TIP. On the other hand, η/s approaches the KSS bound for TDP. At $T_0 = 170$ MeV, we find a typical value for the ratio of $\eta/s = 0.29$ in our present model.

(iv) Our numerical results of η/s for TDP are well comparable with other theoretical estimations, such as the NJL model, LQCD, and χPT for $T = (100 \sim 350)$ MeV. However, we fail to reproduce the values from LQCD and pQCD at very high T. This is not surprising since the present model is well applicable for the low-energy regions only. We also parametrize the numerical result of η/s in a simple polynomial form as a function of $t = T/T_0$ for $B = 0$.

Encouraged by our results obtained here—which agree well with the empirical data—we would like to extend our study to other QGP transport coefficients, such as the bulk viscosity and the heat conductivity [46–48]. Moreover, it would be interesting to take into account the external electric field, which turns out to be considerably strong in heavy-ion collisions. Thus, the external electric field may cause considerable change in the transport coefficients. We also note that if the *inverse* magnetic catalysis—shown in the recent LQCD simulations at finite T [49–52]—is taken into account the sea-quark contributions (as a backreaction from the quarks to the non-Abelian gauge fields) in the present conclusion about the decrease of the shear viscosity in the presence of the magnetic field is likely to be changed. To include this mechanism in our model is very challenging and it is obviously out of the scope of this article. The related works are in progress and will appear elsewhere.

ACKNOWLEDGMENTS

The authors thank S. Cho (Yonsei University) and S.-Y. Wu (NCTU) for fruitful discussions. S.-i. N. is grateful to the warm hospitality during his stay at National Center for Theoretical Science (NCTS, north) of Taiwan, where the present work was partially performed. He also acknowledges the financial supports from NCTS for his stay. The work of C.-W. K. was supported by the Grant No. NSC 99-2112-M-033-004-MY3 from National Science Council (NSC) of Taiwan. He also acknowledges the support of NCTS (North) of Taiwan. The numerical calculations were carried out in part using ABACUS2 computing server at KIAS.

APPENDIX

The quark spectral function is normalized as follows:

$$\frac{1}{2\pi}\int_{-\infty}^{\infty}\rho_{\mathrm{FW}}(w,\boldsymbol{k})dw = \int_{-\infty}^{\infty}\frac{\mathrm{sgn}(w)(w\gamma_0-\alpha)}{2\sqrt{2\pi}E\Lambda}\left[\exp\left[-\frac{(w-E)^2}{2\Lambda^2}\right]+\exp\left[-\frac{(w+E)^2}{2\Lambda^2}\right]\right]dw$$
$$= \int_{-\infty}^{\infty}\frac{\mathrm{sgn}(w)(w\gamma_0-\alpha)}{2\sqrt{2\pi}E\Lambda}\left[\exp\left[-\frac{(w-E)^2}{2\Lambda^2}\right]+\exp\left[-\frac{(w+E)^2}{2\Lambda^2}\right]\right]dw. \tag{A1}$$

Replacing the integral variable as $w \pm E \equiv w_\pm$, Eq. (A1) is led to

$$\int_{-\infty}^{\infty}\left\{\frac{\mathrm{sgn}(w_+-E)[(w_+-E)\gamma_0-\alpha]}{2\sqrt{2\pi}E\Lambda}\exp\left[-\frac{w_+^2}{2\Lambda^2}\right]+\frac{\mathrm{sgn}(w_-+E)[(w_-+E)\gamma_0-\alpha]}{2\sqrt{2\pi}E\Lambda}\exp\left[-\frac{w_-^2}{2\Lambda^2}\right]\right\}dw$$
$$= \frac{\mathrm{sgn}(-E)(-E\gamma_0-\alpha)}{2E}+\frac{\mathrm{sgn}(E)(E\gamma_0-\alpha)}{2E} = \frac{-(-E\gamma_0-\alpha)}{2E}+\frac{+(E\gamma_0-\alpha)}{2E} = \gamma_0, \tag{A2}$$

which satisfies the spectral-function normalization condition.

[1] H. Song, S. A. Bass, U. Heinz, T. Hirano, and C. Shen, Phys. Rev. Lett. **106**, 192301 (2011); **109**, 139904(E) (2012).
[2] G. Policastro, D. T. Son, and A. O. Starinets, Phys. Rev. Lett. **87**, 081601 (2001).
[3] A. Buchel and J. T. Liu, Phys. Rev. Lett. **93**, 090602 (2004).
[4] I. Arsene *et al.* (BRAHMS Collaboration), Nucl. Phys. **A757**, 1 (2005).
[5] P. Kovtun, D. T. Son, and A. O. Starinets, Phys. Rev. Lett. **94**, 111601 (2005).
[6] B. I. Abelev *et al.* (STAR Collaboration), Phys. Rev. C **79**, 034909 (2009).
[7] B. Schenke, P. Tribedy, and R. Venugopalan, Phys. Rev. Lett. **108**, 252301 (2012).
[8] H. Song, Nucl. Phys. **A904–A905**, 114c (2013).
[9] S. Cremonini, Mod. Phys. Lett. B **25**, 1867 (2011).
[10] M. E. Carrington, D. F. Hou, and R. Kobes, Phys. Rev. D **62**, 025010 (2000).
[11] T. Fukutome and M. Iwasaki, Prog. Theor. Phys. **119**, 991 (2008).
[12] J. W. Chen and E. Nakano, Phys. Lett. B **647**, 371 (2007).
[13] J. W. Chen, H. Dong, K. Ohnishi, and Q. Wang, Phys. Lett. B **685**, 277 (2010).
[14] P. B. Arnold, G. D. Moore, and L. G. Yaffe, J. High Energy Phys. 05 (2003) 051.
[15] P. B. Arnold, G. D. Moore, and L. G. Yaffe, J. High Energy Phys. 11 (2000) 001.
[16] X. G. Huang, M. Huang, D. H. Rischke, and A. Sedrakian, Phys. Rev. D **81**, 045015 (2010).
[17] M. Iwasaki, H. Ohnishi, and T. Fukutome, J. Phys. G **35**, 035003 (2008).
[18] X. G. Huang and T. Koide, Nucl. Phys. **A889**, 73 (2012).
[19] C. Sasaki and K. Redlich, Nucl. Phys. **A832**, 62 (2010).
[20] R. Green-Kubo, J. Phys. Soc. Jpn. **12**, 570 (1957).
[21] H. B. Meyer, Phys. Rev. D **76**, 101701 (2007).
[22] K. A. Mamo, J. High Energy Phys. 10 (2012) 070.
[23] A. Bzdak and V. Skokov, Phys. Lett. B **710**, 171 (2012).
[24] K. Tuchin, arXiv:1301.0099.
[25] K. Fukushima, D. E. Kharzeev, and H. J. Warringa, Phys. Rev. D **78**, 074033 (2008).
[26] J. K. Boomsma and D. Boer, Phys. Rev. D **81**, 074005 (2010).
[27] D. Diakonov, Prog. Part. Nucl. Phys. **51**, 173 (2003).
[28] T. Schafer and E. V. Shuryak, Phys. Rev. D **53**, 6522 (1996).
[29] B. J. Harrington and H. K. Shepard, Nucl. Phys. **B124**, 409 (1977).
[30] D. Diakonov and A. D. Mirlin, Phys. Lett. B **203**, 299 (1988).
[31] S.-i. Nam, J. Phys. G **37**, 075002 (2010).
[32] J. S. Schwinger, Phys. Rev. **82**, 664 (1951).
[33] J. F. Nieves and P. B. Pal, Phys. Rev. D **73**, 105003 (2006).
[34] S.-i. Nam, H.-Y. Ryu, M. M. Musakhanov, and H.-Ch. Kim, J. Korean Phys. Soc. **55**, 429 (2009).
[35] O. Espinosa, Phys. Rev. D **71**, 065009 (2005).
[36] M. C. Chu, J. M. Grandy, S. Huang, and J. W. Negele, Phys. Rev. D **49**, 6039 (1994).
[37] E. V. Shuryak, Nucl. Phys. **B203**, 93 (1982).
[38] S.-i. Nam and H.-Ch. Kim, Phys. Lett. B **666**, 324 (2008).
[39] T. Schafer and E. V. Shuryak, Rev. Mod. Phys. **70**, 323 (1998).
[40] K. Goeke, M. M. Musakhanov, and M. Siddikov, Phys. Rev. D **76**, 076007 (2007)
[41] S.-i. Nam (to be published).
[42] S.-i. Nam and C.-W. Kao, Phys. Rev. D **83**, 096009 (2011).
[43] V. A. Miransky and I. A. Shovkovy, Phys. Rev. D **66**, 045006 (2002).
[44] A. Nakamura and S. Sakai, Phys. Rev. Lett. **94**, 072305 (2005).
[45] Z. Xu and C. Greiner, Phys. Rev. Lett. **100**, 172301 (2008).
[46] K. Fukushima, Phys. Lett. B **591**, 277 (2004).
[47] C. Ratti, M. A. Thaler, and W. Weise, Phys. Rev. D **73**, 014019 (2006).
[48] S.-i. Nam, Phys. Rev. D **86**, 033014 (2012).
[49] G. S. Bali, F. Bruckmann, G. Endrődi, Z. Fodor, S. D. Katz, S. Krieg, A. Schäfer, and K. K. Szabó, J. High Energy Phys. 02 (2012) 044.
[50] G. S. Bali, F. Bruckmann, G. Endrodi, Z. Fodor, S. D. Katz, and A. Schafer, Phys. Rev. D **86**, 071502 (2012).
[51] G. S. Bali, F. Bruckmann, G. Endrodi, F. Gruber, and A. Schaefer, J. High Energy Phys. 04 (2013) 130.
[52] F. Bruckmann, G. Endrodi, and T. G. Kovacs, J. High Energy Phys. 04 (2013) 112.